

Absorption and scattering properties of nanoparticles in an absorbing medium: revisiting with experimental validation

Pham Thi Hong

*Nano and Energy Center, VNU University of Science, Vietnam National University,
120401 Hanoi, Vietnam*

Nguyen Trung Kien

*Nano and Energy Center, VNU University of Science, Vietnam National University,
120401 Hanoi, Vietnam*

Nguyen Viet Tuyen

*Faculty of Physics, VNU University of Science, Vietnam National University, 120401
Hanoi, Vietnam*

Hung Q. Nguyen

*Nano and Energy Center, VNU University of Science, Vietnam National University,
120401 Hanoi, Vietnam*

H. T. M. Nghiem

Phenikaa Institute for Advanced Study, Phenikaa University, 12116 Hanoi, Vietnam

Abstract

Absorption and scattering properties of nanoparticles immersed in an absorbing medium are essential in understanding the overall properties of composites and in designing materials with expected functionalities. In this paper, we establish the model that links the absorption and scattering coefficients of individual particles with the reflectance and transmittance spectra of thin-film composite, supported by well-controlled experiments. Thin films consisting of TiO_2 nanoparticles embedded in PMMA are fabricated on glass substrates using spin-coating and then peeled off to form standalone samples for spectroscopy measurements. The absorption K and scattering S coefficients of multiple nanoparticles are calculated from the measured transmittance and reflectance using the Kubelka-Munk theory in combination with the Saunderson correction. From the theoretical side, the absorption K and scattering S coefficients are the accumulation

Email address: `hoa.nghiemthimin@phenikaa-uni.edu.vn` (H. T. M. Nghiem)

of absorption and scattering of individual particles, which are derived from the Mie theory. The agreement between the K and S coefficients extracted from experimental data and from theoretical calculations gives deep insight into the significant attenuating effect of absorption and scattering on each particle due to the surrounding medium. Furthermore, the validated model of nanoparticles immersed in an absorbing medium can be used to obtain the preliminary results for materials designed toward radiative cooling.

Keywords: Mie theory of nanoparticles in an absorbing medium, Kubelka-Munk theory, thin-film composite, scattering coefficient, absorption coefficient, radiative cooling.

1. Introduction

Nanoparticles hold vast applications as being immersed in polymers due to their ability to actively interact with the environments and therefore modify the host properties [1] such as reinforcing the polymer matrix [2, 3], stabilizing the thermal properties together with retarding flame [4, 5, 6], lifting the barrier of polymer to enhance the gas and liquid resistance [7, 8], varying how light transmitting in polymer [9, 10], preventing the growth of bacteria and other microorganisms [11, 12], changing electrical properties toward electrical conducting, sensing or catalysis [13, 14, 15]. Among those, optical properties can be used for applications in radar [16], metamaterials [17, 18], or passive cooling [19]. A typical polymer exhibits intense radiation in the mid and far infrared range due to the vibration and stretching of its organic constituents [20]. Recent studies also suggest that polymers absorb in the UV regime [21, 22]. In this paper, we are interested in using nanoparticles to modify the optical properties of a polymer in the UV-VIS-NIR regime.

The overall optical properties of thin-film composites depend on the basic optical parameters of their components. Within the Kubelka-Munk theory, considering the fraction of reflected light at the front interface and that of transmitted light through the back interface, the two significant parameters are the absorption K and scattering S coefficients of the total particles [23]. Therefore, one can build up a procedure to extract these coefficients from measured data of transmitted and reflected light, following the step in the left-direction arrow in Fig. 1. In the case of regular-transmittance, one can get the extinction coefficients of the total particles, not the absorption and scattering coefficients separately [24, 25]. While, with the use of both the total, regular and diffuse, transmittance and total reflectance, the K and S coefficients can be extracted within the two-flux Kubleka-Munk theory combined with Saunderson correction [26, 27, 28, 29]. On the other hand, the explicit connection between the Kubleka-Munk coefficients and the optical properties of individual particles is brought up by the use of radiative transfer equations [30, 31, 32, 33]. As a result, the absorption K and scattering S coefficients are defined as the accumulation of absorption and scattering of individual particles, which are calculated using Mie theory [34]. Hence, one can complete the forward procedure for the

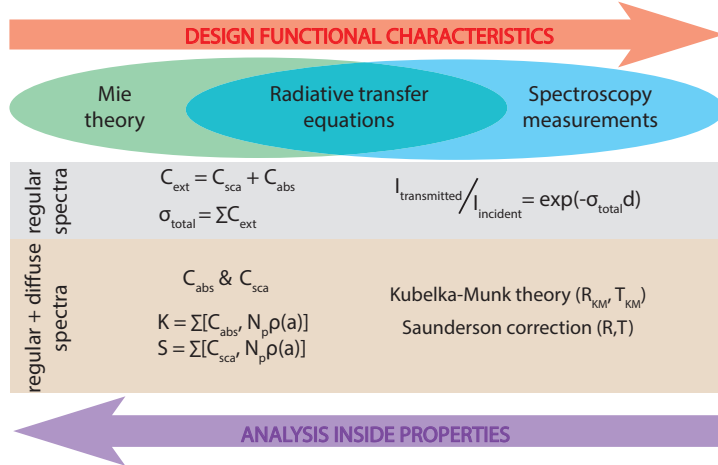


Figure 1: **The relation between theoretical calculation and experimental observation** in optical properties of thin-film composites. The two-way mapping shows the possibility of component analysis in one way - the violet arrow direction and the prediction of composite functionality in the reversed way - the red arrow direction.

prediction of thin-film composite optical properties from the individual particles, described as the right-direction arrow in Fig. 1. In general, the calculation of Mie cross-sections is more common in a non-absorbing medium than in an absorbing medium [34, 35, 36]. Since the polymer strongly absorbs in the ultraviolet and infrared regions [20, 21, 22], the contribution of the medium to the optical properties of the particles must be considered. This problem is solved by assuming an individual particle embedded in the absorbing medium as a coated particle with an effective radius. In the early studies [37, 38, 39], the problem is mainly solved with the far-field approximation in which the effective radius larger than the incoming wavelength. The latter study provides detailed expressions for the absorption and scattering cross-sections of a single particle with an arbitrary effective radius [40]. The similar expressions are also shown in the other studies [41, 42]; however, the effective radius is set to be equal to the particle radius.

In this work, we determine the absorption K and scattering S coefficients of thin-film composites from two approaches: extracting from measured data and calculating from theory, as represented by two big arrows in Fig. 1. We fabricate the thin-film composites consisting TiO_2 nanoparticles embedded in PMMA and then measure their overall optical properties. From the measured data, the K and S coefficients are extracted within Kubelka-Munk theory and Saunderson correction following the left-direction arrow in Fig. 1. In the theoretical calculation, the K and S coefficients accumulate the absorption and scattering of individual particles. In our previous report [22], we notice that PMMA absorbs in the ultraviolet and near-infrared regions. Therefore, in this paper, we calculated the optical properties of single particles within Mie the-

Name	Log-norm distribution			
	mean (nm)	mode (nm)	μ (nm)	σ (nm)
M15	15	6.75	2.44	0.72
M55	55	35	3.86	0.55

Table 1: **Parameters of the TiO_2 nanoparticle size distribution**, the log-normal function $\rho(a) = \frac{1}{a\sigma\sqrt{2\pi}} \exp\left(-\frac{(\ln a - \mu)^2}{2\sigma^2}\right)$. The mean and mode of TiO_2 nanoparticles dispersed in water are measured using the Zetasizer nano S from Malvern Panalytical.

ory, specified for an absorbing medium and an arbitrary effective radius [40]. The test cases for the effective radius are: i) the effective radius equal to half the sample thickness, and ii) the effective radius equal to the particle radius. The comparison between the experimental data and theoretical results shows that the test case i) is more preferable than the test case ii). This proves the significant attenuating effect of absorption and scattering on each particles due to the surrounding medium. Within the confirmed theory, we proceed to make forward predictions for the optical properties of some thin-film composites, as indicated by the right-direction arrow in Fig. 1.

2. Experimental and Theoretical Methods

2.1. Sample Fabrication

We use TiO_2 nanoparticles and PMMA polymer to fabricate the thin-film composite. The PMMA obtained from Sumitomo Chemical Co. is in granular form with a molecular weight of 1.18 g/cm^3 [43]. TiO_2 nanoparticles with purity of 99.8% are obtained from Shanghai Aladdin Bio-Chem Technology. The sizes of TiO_2 particles dispersed in a water medium are measured with a dynamic light scattering apparatus using the ZetaSizer Nano S analyzer (presented in section 1, supplementary). The mean and mode values of particle radius are presented in the second and third columns in table 1. The mean radii for the two types of TiO_2 nanoparticles are 15 nm and 55 nm, denoted as M15 and M55, respectively. Throughout the paper, the corresponding series of samples are labeled as M15 and M55. From measured mean and mode values, the parameters of the particle size distribution, μ and σ , are determined as shown in table 1.

The thin-film composites of Poly(Methyl Methacrylate) polymer (PMMA) with titanium dioxide nanoparticles (TiO_2) are fabricated in our cleanroom using spin-coating. Initially, PMMA is dissolved in acetone at a ratio of 1:8. After that, TiO_2 nanoparticles are added into the mixture and magnetic stirred for 5 hours until uniformly distributed. The mixture of PMMA and TiO_2 is spin-coated at 300 rpm in 3 minutes using a standard spin-coater on a glass substrate size $2.54 \times 2.54 \text{ cm}^2$. Since acetone evaporates quite fast, the sample dries on itself without any baking steps. Two series of samples M15 and M55

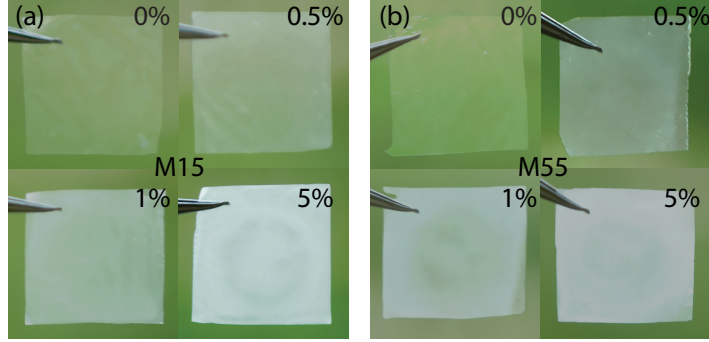


Figure 2: **Morphology of thin-film composites:** The pictures of the standalone films with four TiO_2 concentrations mixing in polymer: 0%, 0.5%, 1%, and 5% in (a) series M15 and in (b) series M55. The sample size is about $2.3 \times 2.3 \text{ cm}^2$. The contrast between samples and green (grey) background linearly changes when particle concentrations increase.

Name	Average sample thickness d (μm)			
	0%	0.5%	1%	5%
series M15	5.1 ± 0.7	5.3 ± 1.1	5.1 ± 0.8	5.5 ± 0.7
series M55	5.8 ± 0.9	6.7 ± 1.2	8.2 ± 2.1	6.3 ± 1.1

Table 2: **Thickness of 8 samples** in series M15 and series M55 with four TiO_2 concentrations: 0%, 0.5%, 1%, and 5%. Sample thicknesses are measured by a KLA Tencor D-100 profilometer.

are fabricated at different TiO_2 concentrations of mass c_m : 0%, 0.5%, 1%, and 5%, respectively. The first set of samples is used to measure the sample thickness using a KLA Tencor D-100 profilometer, as shown in Table 2. These data are used as the input parameters for later calculations, as presented in the following sections. The second set of samples is peeled off from their glass substrates with the help of copper tapes. These standalone films are used for optical measurements, which provide total transmittance and total reflectance data. Being fabricated simultaneously with the identical recipe, these two sets of samples are supposed to have the same morphological structures and optical properties. Images of standalone thin films in series M15 and series M55 are shown in Fig. 2a and Fig. 2b, respectively.

Optical properties of thin-film composites are measured in the wavelength from 0.2 to $2.5 \mu\text{m}$. The total transmittance and total reflectance spectra of the standalone thin-film composites are obtained using the Hitachi UH-4150 system with an integrating sphere. We skip the data in the region from 0.8 to $0.9 \mu\text{m}$ due to a switch in the detector near $0.85 \mu\text{m}$ that leads to noisy data. Fig. 3a and Fig. 3d present the total transmittance of thin-film composites of series M15 and series M55, respectively, with four different mass concentrations of TiO_2 nanoparticles: 0% in black, 0.5% in green, 1% in red, and 5% in purple. The total reflectance of series M15 and M55 are shown in Fig. 3b and Fig. 3e,

respectively. They removed the effect of BaSO_4 substrate as presented in detail in our previous report [22]. From T and R , the total emittance E of thin films are determined by $E = 1 - T - R$, as shown in Fig. 3c of series M15 and Fig. 3f of series M55. The optical properties of both series follow the mass concentrations of TiO_2 nanoparticles linearly.

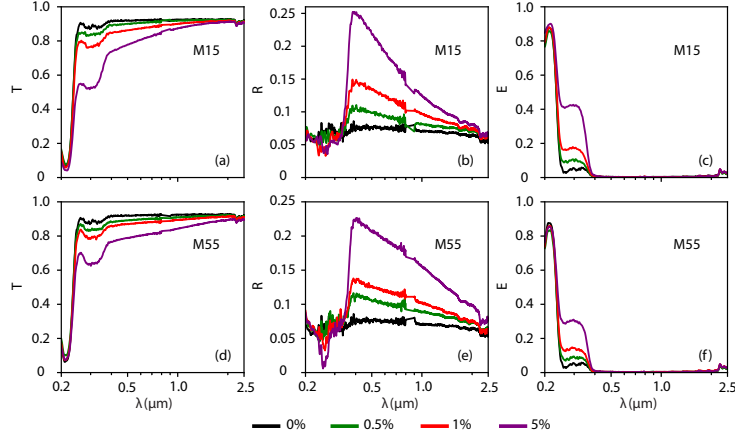


Figure 3: **UV-Vis-NIR spectra of thin-film composites.** The total transmittance T is in (a) and (d), and the total reflectance R is in (b) and (e) of series M15 and series M55, respectively. While, the total emittance E is calculated by $E = 1 - T - R$ in (c) and (f). Each series has four samples with different mass concentrations: 0% in black, 0.5% in green, 1% in red, and 5% in purple.

2.2. The Two-flux Kubelka-Munk Method and Saunderson Correction for Thin-film Composites

The two-flux Kubelka-Munk theory is a standard approach that describes light propagation in thin-film composites. The model is formulated using two differential equations for radiation fluxes flowing in both forward and backward directions within the medium [23]. The intensities of two radiation fluxes depend on the film thickness d , the absorption coefficient K , and the scattering coefficient S . Solving these equations allows us to determine the reflectance and transmittance of the thin-film composite as shown in Fig. 4a [23, 44], which are

$$R_{\text{KM}} = \frac{1 - R_g[A - B \coth(BSd)]}{A - R_g + B \coth(BSd)}, \quad (1)$$

$$T_{\text{KM}} = \frac{B(1 - R_g)}{(A - R_g) \sinh(BSd) + B \cosh(BSd)}, \quad (2)$$

in which R_g is the backside internal reflectance of the film. A and B are parameters related to the scattering and absorption coefficients

$$A = \frac{K + S + K_p}{S}, \quad (3)$$

$$B = \sqrt{A^2 - 1}, \quad (4)$$

with $K_p = 4\pi\kappa_h/\lambda$, in which κ_h is the extinction coefficient of the host medium and λ is the light wavelength. However, the two-flux Kubelka-Munk theory does not consider the reflection losses at the frontside boundaries. The problem is solved using the Saunderson correction. The total reflectance R and the total transmittance T , respectively represented by the red and purple arrows at the boundaries in Fig. 4a, are expressed by [45]

$$R = R_c + \frac{(1 - R_c)(1 - R_j)R_{KM}}{1 - R_j R_{KM}}, \quad (5)$$

$$T = \frac{(1 - R_c)T_{KM}}{1 - R_j R_{KM}}. \quad (6)$$

The reflections at the frontside boundaries are R_c and R_j . R_c indicates the fraction of collimated light reflected at the front interface, while R_j depends on the fraction of light diffused, q_j , inside the materials such that $R_j = (1 - q_j)R_c + q_jR_d$, in which R_d indicates the reflection of diffused light. Similarly, $R_g = (1 - q_g)R_c + q_gR_d$ (presented in section 2, supplementary). Using the equations 1-6, we can invert the absorption K and scattering S coefficients from the total transmittance T and total reflectance R .

2.3. Absorption and Scattering Properties of a Single Particle

In the limit of small particle density N_p , the absorption K coefficient and scattering S coefficient in the two-flux Kubelka-Munk theory are the accumulation of the absorption and scattering cross-sections of individual particles [30, 31, 32, 33], as shown in Fig. 4b. With a continuous distribution of particle size $\rho(a)$, K and S are calculated by

$$K = 2N_p \int \rho(a)C_{abs}da, \quad (7)$$

$$S = \frac{3}{4}N_p \int (1 - g)\rho(a)C_{sca}da, \quad (8)$$

in which g is the anisotropy factor [31, 32, 33]. The absorption and scattering cross-sections of individual particles, C_{abs} and C_{sca} , are calculated within Mie theory.

When particles are placed in an absorbing medium, the effect of the surrounding medium on the absorption and scattering coefficient of individual particles is significant. To solve this problem, Ref. [40] and Ref. [41] focus on the coordinate bodies with different physical properties to determine the Mie cross-sections. Ref. [40] assumes that a particle embedded in an absorbing medium

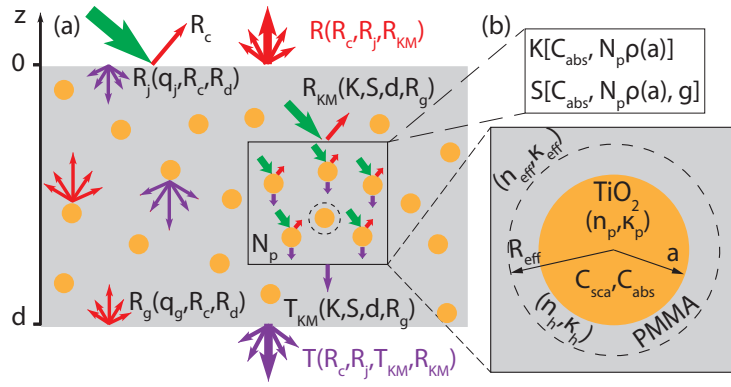


Figure 4: **Schematic model of thin-film composite under light exposure:** (a) Optical paths of light and (b) Theoretical model for the absorption K and scattering S coefficients of particles. In (a), R_c is the fraction of collimated light reflection at the front interface, while R_d indicates the reflection of diffused light. R_j and R_g are the frontside and backside internal reflectance of the thin-film composite depending on the fraction of light diffused, q_j and q_g , respectively (presented in section 2, supplementary). R_{KM} and T_{KM} are Kubelka-Munk reflectance and transmittance determined by equation 1 and equation 2. The overall optical properties of the thin-film composite are expressed by the total reflectance R in equation 5 and total transmittance T in equation 6. In (b), the values K and S are the accumulation of absorption and scattering of individual particles in equation 7 and equation 8. Absorbing cross-sections C_{abs} and scattering cross-section C_{sca} are determined within Mie theory in following equations 9-13. TiO_2 particles (n_p, κ_p) embedded in $PMMA$ medium (n_h, κ_h) are assumed as a coated particle with an effective radius R_{eff} in the host medium (n_{eff}, κ_{eff}).

becomes a coated particle with inner radius a and outer effective radius R_{eff} . The Mie cross-sections for an arbitrary particle size are expressed as follows,

$$\begin{aligned}
C_{\text{ext}} = & -\frac{2\pi}{|k|^2} \sum_{l=1}^{\infty} (2l+1) \times \{ \text{Re}(a_l + b_l) \text{Im}(\xi_l(kR_{\text{eff}}) \psi_l^{*'}(kR_{\text{eff}}) \\
& - \xi_l'(kR_{\text{eff}}) \psi_l^*(kR_{\text{eff}})) + \text{Im}(a_l + b_l) \text{Re}(\xi_l(kR_{\text{eff}}) \psi_l^{*'}(kR_{\text{eff}}) \\
& - \xi_l'(kR_{\text{eff}}) \psi_l^*(kR_{\text{eff}})) + \frac{\text{Im}(k)}{\text{Re}(k)} \text{Re}(a_l - b_l) \text{Re}(\xi_l(kR_{\text{eff}}) \psi_l^{*'}(kR_{\text{eff}}) \\
& + \xi_l'(kR_{\text{eff}}) \psi_l^*(kR_{\text{eff}})) - \frac{\text{Im}(k)}{\text{Re}(k)} \text{Re}(a_l - b_l) \text{Im}(\xi_l(kR_{\text{eff}}) \psi_l^{*'}(kR_{\text{eff}}) \\
& + \xi_l'(kR_{\text{eff}}) \psi_l^*(kR_{\text{eff}})) \}, \tag{9}
\end{aligned}$$

$$\begin{aligned}
C_{\text{sca}} = & -\frac{2\pi}{|k|^2} \sum_{l=1}^{\infty} (2l+1) \times \{ (|a_l|^2 + |b_l|^2) \text{Im}(\xi_l(kR_{\text{eff}}) \xi_l^{*'}(kR_{\text{eff}})) \\
& + \frac{\text{Im}(k)}{\text{Re}(k)} (|a_l|^2 - |b_l|^2) \text{Re}(\xi_l(kR_{\text{eff}}) \xi_l^{*'}(kR_{\text{eff}})) \}, \tag{10}
\end{aligned}$$

$$C_{\text{abs}} = C_{\text{ext}} - C_{\text{sca}}, \tag{11}$$

where ψ_l and ξ_l are the Riccati-Bessel functions. $k = 2\pi(n_h + i\kappa_h)/\lambda$, in which $n_h + i\kappa_h$ is the refractive index of host medium. a_l and b_l are Mie coefficients [34],

$$a_l = \frac{m\psi_l(mx)\psi_l'(x) - \psi_l(x)\psi_l'(mx)}{m\psi_l(mx)\xi_l'(x) - \xi_l(x)\psi_l'(mx)}, \tag{12}$$

$$b_l = \frac{\psi_l(mx)\psi_l'(x) - m\psi_l(x)\psi_l'(mx)}{\psi_l(mx)\xi_l'(x) - m\xi_l(x)\psi_l'(mx)}, \tag{13}$$

where $x = ka$ is the size parameter, $m = (n_p + i\kappa_p)/(n_h + i\kappa_h)$, and $n_p + i\kappa_p$ is the refractive index of particle. Thin-film composite, including the particles immersed in a polymer medium, becomes a particulate environment with the refractive index $(n_{\text{eff}} + i\kappa_{\text{eff}})$ [46]. It represents the mean effect of other particles inside the composite on a given particle (presented in section 4, supplementary). Thus, we replace $(n_h + i\kappa_h)$ by $(n_{\text{eff}} + i\kappa_{\text{eff}})$ in equations 9-13 as using the Mie cross-sections of a single particle to calculate the total absorption and scattering coefficients of all the particles, equations 7 and 8.

Other studies [41, 42] also examine the optical properties of single particles in an absorbing medium with similar expressions as in Ref. [40]; however, the effective radius is equal to the particle radius. In this paper, we calculate the Mie cross-sections in the two cases: $R_{\text{eff}} = d/2$ and $R_{\text{eff}} = a$. After that, the comparison of the theoretical result and experimental data evaluates the suitable theory to determine the K and S coefficients of nanoparticles in an absorbing medium.

Name	Diffuse light fraction q_g		
	0.5%	1%	5%
series M15	0.127	0.245	0.5
series M55	0.069	0.169	0.5

Table 3: **Fraction of light diffused at front interface** q_g with three concentrations: 0.5%, 1% and 5% of series M15 and M55. We assume that the fraction of light diffused at the back interface $q_j = 2q_g$, which imposes a maximum value for $q_g \leq 0.5$.

3. Results and Discussion

3.1. K - S extracted from experiments

Fig. 5 shows the absorption and scattering coefficients of particles extracted from measured data by inverting equations 1-6. The fractions of light diffused are necessary to determine the internal reflection of the film at both interfaces R_j and R_g . The fraction of light diffused at the back interface, q_g , is defined by the total particle cross-section in the unit of sample area. The fraction of light diffused at the front interface is assumed to be $q_j = 2q_g$, therefore the maximum value of q_g is equal to 0.5. Following these points, the fractions of light diffused for each series of samples are presented in Table 3. These values fall within the reasonable ranges of q_g and q_j , ensuring that the total $K + S$ extracted from experiments remains physically non-negative (section 3, supplementary).

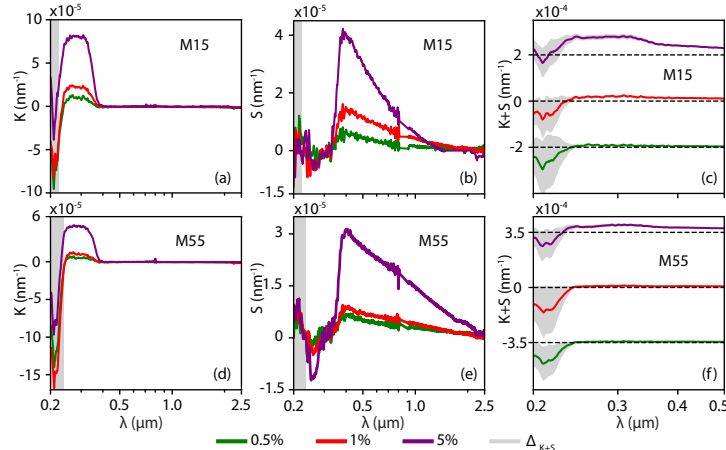


Figure 5: **(Color online) K - S extraction from measured data:** series M15 in (a) and (b), series M55 in (d) and (e). The K - S values are determined by inverting equations 1-6 in the wavelength range from 0.2 to 2.5 μm with three mass concentrations of 0.5% in green, 1% in red, and 5% in purple, respectively. The uncertainty of $(K + S)$ in gray area determined by equation 14 is presented in (c) for series M15 and in (f) for series M55.

The absorption coefficient of TiO_2 nanoparticles in series M15 and series M55 are shown in Fig. 5a and Fig. 5d with three mass concentrations: 0.5% in

green, 1% in red, and 5% in purple, respectively. Since TiO_2 strongly absorbs in the ultraviolet region (presented in Fig.S3b, section 3, supplementary), the absorption K coefficients of TiO_2 nanoparticles linearly increase following the TiO_2 mass concentrations in the wavelength range of $0.24 - 0.38 \mu\text{m}$, while they are approximately zero in the visible and near-infrared region. However, K strongly decays at $\lambda < 0.24 \mu\text{m}$ due to the strong absorption of the medium in this range. This point is made clear with the comparison to the theoretical results in the following subsection. Fig. 5b and Fig. 5e respectively present the scattering coefficient S of series M15 and series M55. The scattering coefficient S strongly depends on the increased mass concentration in the visible and near-infrared regions and weakly changes in the ultraviolet region.

In extracting K and S of TiO_2 nanoparticles, the accuracy of our final results depends on the sample, and, in this paper, it mainly depends on the sample thickness. Analysing the uncertainty of the total $K + S$ from equations 1 and 2 [47], we have

$$\Delta_{K+S} \approx \frac{|K + S + K_p| \Delta d}{d}, \quad (14)$$

where Δd is the error in thickness measurement, presented in Table 2. From $K + S \pm \Delta_{K+S}$ expressed through gray areas in Fig. 5c for the series M15 and Fig. 5f for the series M55, we define the unreliable range such that $(K + S + \Delta_{K+S})$ is negative. We use gray rectangles to annotate the unreliable range in the following figures.

3.2. K - S calculated from theory

Using the theoretical model in subsection 2.3, we calculate the absorption K coefficient and scattering S coefficient of particles in an absorbing medium. From the effective refractive index of host medium ($n_{\text{eff}} + i\kappa_{\text{eff}}$), the refractive index of particle ($n_p + i\kappa_p$), and the particle density N_p , the values of K - S are determined using equations 7-13. These refractive indices are presented in section 4, supplementary. The particle density N_p is given by

$$N_p = \frac{c_m(d_{\text{PMMA}}/d_{\text{TiO}_2})/(1 + c_m d_{\text{PMMA}}/d_{\text{TiO}_2})}{\int \frac{4}{3}\pi a^3 \rho(a) da}, \quad (15)$$

where d_{PMMA} and d_{TiO_2} are the specific masses of PMMA and TiO_2 respectively. Based on the theoretical calculation model in subsection 2.3, we calculate the K and S coefficients of TiO_2 nanoparticles in PMMA in the two test cases: $R_{\text{eff}} = d/2$ and $R_{\text{eff}} = a$. The comparison between the K and S coefficients calculated from theory and extracted from experiments evaluates the effect of the absorbing medium on the optical properties of nanoparticles.

In the first test case, the absorption K and scattering S coefficient of TiO_2 nanoparticles in PMMA are calculated with $R_{\text{eff}} = d/2$, as present in Fig. 6. The top row in Fig. 6 shows the K and S of series M15, while the bottom row in Fig. 6 presents that of series M55 with three the mass concentration. The results of theoretical calculations are shown in dashed lines, while experimental data are

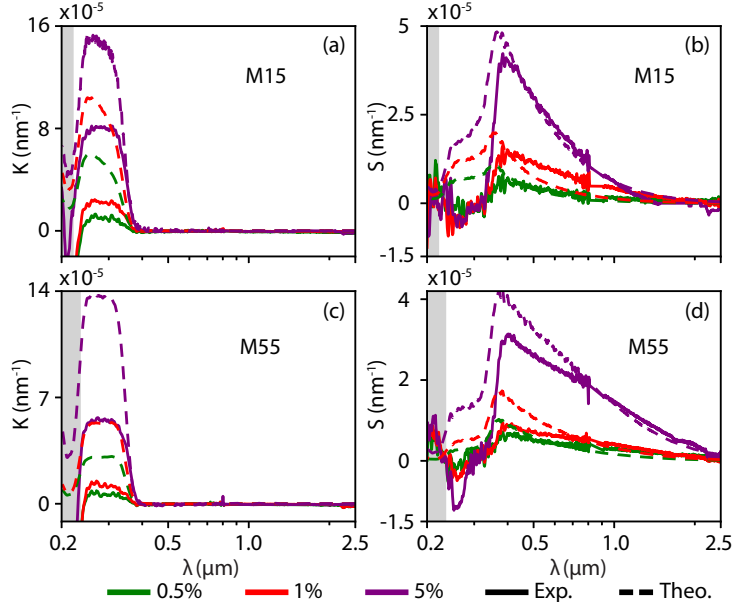


Figure 6: (Color online) Comparison between theoretical and experimental results (K, S) in the $R_{\text{eff}} = d/2$ case: series M15 in (a) and (b), series M55 in (c) and (d). The theoretical values of K and S are computed using equations 7-13 with the contribution of the absorbing medium in the optical properties of immersed particles as in Ref.[40]. In which d is the sample thickness with three mass concentrations: 0.5% in black, 1% in green, and 5% in purple.

in solid lines. In this case, the spectra K calculated from the theory in Fig. 6a of series M15 and Fig. 6c of series M55 express the trend of the experimental data of both series. The optical properties of the TiO_2 nanoparticles depend on the concentration and type of TiO_2 particles together with the characterization of PMMA at different wavelengths. Since PMMA has the highest absorption at $\lambda = 0.22\mu\text{m}$ (presented in Fig. S3a in section 3, supplementary), it makes the absorption coefficient K of TiO_2 nanoparticles no full absorption as TiO_2 bulk at $\lambda \leq 0.24\mu\text{m}$. It means that the absorbing medium affects the optical properties of TiO_2 nanoparticles. Similarly, the S coefficient calculated from the theory and extracted from the experiment match well, as shown in Fig. 6b of series M15 and Fig. 6d of series M55. The magnitude of $K-S$ between the theory and experiment of series M55 differs more than that of series M15. This is because the large particles settle more quickly than small ones, so they can not be inspected by the laser light source in the particle size measurement. Although the accuracy measurement of input data affects the theoretical results, calculations based on Ref. [40] produce K and S with values closely matching the measurement data.

In the second test case, the K and S coefficients are calculated in the case of the effective radius equaling the particle radius, $R_{\text{eff}} = a$. Similar to the above

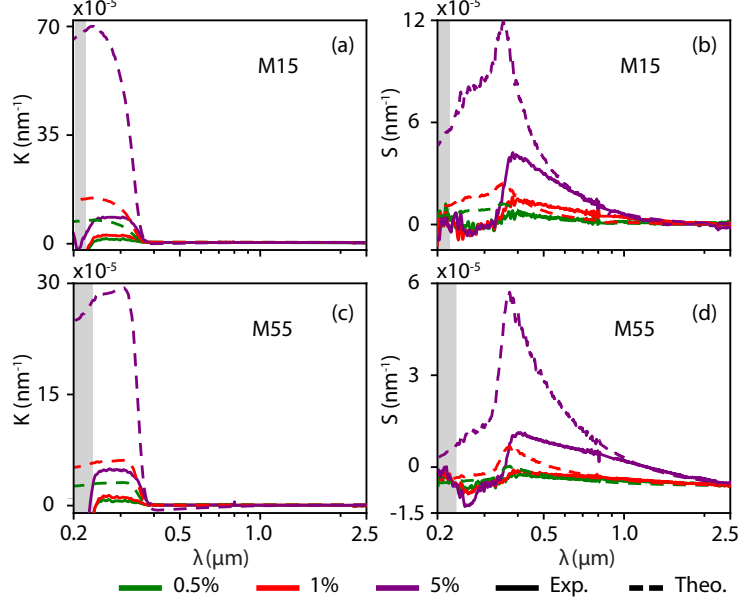


Figure 7: (Color online) Comparison between theoretical and experimental results (K, S) in the $R_{\text{eff}} = a$ case: series M15 in (a) and (b), series M55 in (c) and (d). The K - S of immersed particles is also calculated by equations 7- 13. The optical properties of immersed particles are calculated equivalent to the theory in Ref. [41].

calculation, we compute the K and S coefficients for series M15 and series M55 as shown in Fig. 7. The theoretical K coefficient in series M15 in Fig. 7a and M55 in Fig. 7c is approximately zero coinciding with the experimental data in the visible and near-infrared regions due to the non-absorbing properties of TiO_2 nanoparticles and the PMMA medium. However, the theoretical K spectra do not exhibit the tendency and the scale of the experimental data in the ultraviolet regime. Likewise, the theoretical S spectra of series M15 in Fig. 7b and series M55 in Fig. 7d do not match with experimental results. Therefore, the weak effect of the absorbing medium presented by Ref. [41] as setting $R_{\text{eff}} = a$ is not suitable in the theoretical $K - S$ calculation of immersed nanoparticles with low particle density. With these comparisons of the theoretical results and experimental data, the first test case of $R_{\text{eff}} = d/2$ is proved to be better than the second test case of $R_{\text{eff}} = a$. This suggests that absorption and scattering on each particle are strongly attenuated by the surrounding medium.

3.3. Forward prediction of the overall properties of thin-film composite

In subsection 3.2, we demonstrate the effect of the absorbing medium on the optical properties of immersed nanoparticles with the reasonable use of $R_{\text{eff}} = d/2$. With these theoretical K - S results, we calculate the overall optical properties of thin-film composite by following equations 1-6. Calculations based

on this theoretical model produce T , R , and E with values closely matching with the measured data as shown in Fig. 8.

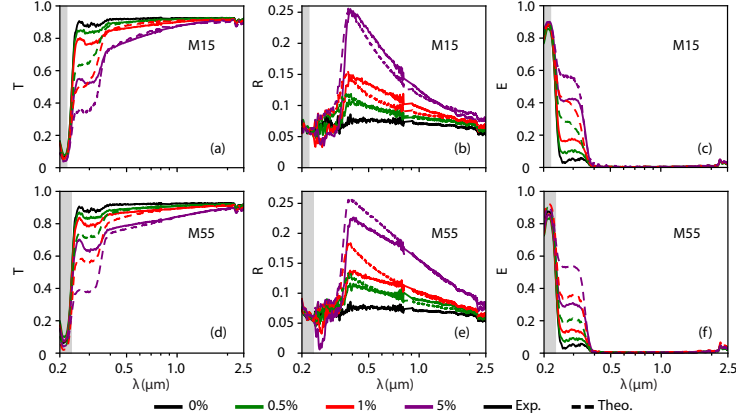


Figure 8: (Color online) Theoretical overall optical properties of thin-film composites (T , R , E): series M15 in (a)-(c), while series M55 in (d)-(f). From the absorption K and scattering S coefficients calculated from theory in the $R_{\text{eff}} = d/2$ case, the total transmittance T and total reflectance R are straightforward by following equations 1-6, while the total emittance E is determined by $E = 1 - T - R$

With the validated model in hand, we make some preliminary calculations for the purpose of materials design toward radiative cooling. For this application, a material is expected to meet two requirements: high solar reflectance ($\lambda \sim 0.3\text{--}2.5\mu\text{m}$) and mid-infrared emittance in the atmosphere transmission window ($\lambda \sim 8\text{--}13\mu\text{m}$) [48, 49]. Even though TiO_2 is commonly used as pigments in reflective paints, it satisfies only a part of the first requirement as showing the enhancement of reflection in the range from $\lambda \sim 0.38\text{--}2.5\mu\text{m}$, as in Figs. 8 (b) and (e). Furthermore, its strong absorption in the UV range, Figs. 8 (c) and (f), may negatively enhance the materials degradation.

To improve the reflectance and reduce the absorption of thin-film composite in these ranges, we replace TiO_2 nanoparticles in the PMMA medium with air bubbles due to its non-absorptive property. The input data, such as the particle sizes, volume concentrations, and sample thickness, is assumed to be the same as the TiO_2 sample series M15 and M55. As shown in Figs. 9a and d, the total transmittance T weakly decreases in comparison with PMMA when increasing the volume concentrations of air bubbles. Especially, in the wide range of $\lambda \sim 0.24\text{--}2.5\mu\text{m}$, the total reflectance R is improved as shown in Figs. 9b and e, and the total absorption of both series does not change with the increasing volume of air in the composite, Figs. 9c and f. The wider range of reflectance and the weaker absorption of thin-film composite with air bubbles than those with TiO_2 shows the potential of using other components to replace TiO_2 toward the application of radiative cooling.

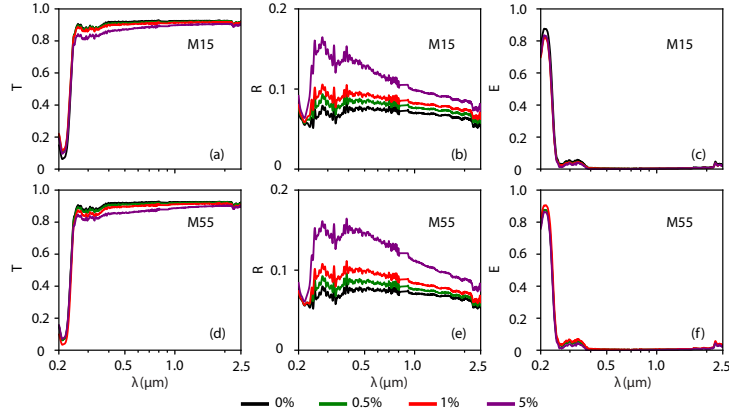


Figure 9: (Color online) **Prediction results of the overall optical properties of air bubble dispersed in PMMA:** (a),(d) the total transmittance T , (b),(e) total reflectance, and (c),(f) the total emittance E of series M15 and series M55, respectively. Replacing the TiO_2 nanoparticles with air bubbles, we predict the overall optical properties of air bubbles in PMMA unchanged the particle sizes, volume concentrations, and sample thickness.

4. Conclusion

In this paper, we study the absorption K and scattering S coefficients of TiO_2 nanoparticles immersed in PMMA medium using both experimental and theoretical methods. Thin-film composites are fabricated by spin-coating and then peeled off to form standalone samples for the spectroscopy measurement. The overall optical properties of thin-film composites are measured using the UV-Vis-NIR spectrophotometer in the wavelength range from 0.2 to $2.5 \mu\text{m}$. Using the Kubelka-Munk theory combined with Saunderson correction, we successfully extract the K and S coefficients from the total transmittance T and total reflectance R . In the theoretical calculation, we validate the theoretical model in Ref. [40] to determine the absorbing and scattering of the nanoparticles immersed in an absorbing medium within Mie theory in the two test cases: $R_{\text{eff}} = d/2$ and $R_{\text{eff}} = a$. Our analysis reveals that the agreement between the experimental and theoretical results is better for the first test case ($R_{\text{eff}} = d/2$) compared to the second test case ($R_{\text{eff}} = a$). This indicates that the absorption and scattering of each particle are strongly attenuated by the surrounding medium. By using the theoretical values of K and S , we recalculate the overall optical properties of the thin-film composites. The theoretical results show good agreement in the scale and tendency of the experimental data.

The validated theory of absorption and scattering of nanoparticles immersed in an absorbing medium is utilized to predict the optical properties of other thin-film composites, i.e., air bubbles dispersed in the PMMA medium. From this, we can outlook using the established model of nanocomposites for fast scanning the optical properties before real experiments, making it a useful tool for designing radiative cooling materials.

Acknowledgments.

This research is funded by Vietnam National Foundation for Science and Technology Development (NAFOSTED) under grant number 103.02-2021.95. Pham Thi Hong was funded by VinBigdata, Vingroup and supported by the Master, PhD Scholarship Programme/PostDoctoral Scholarship Programme of Vingroup Innovation Foundation (VINIF), Vingroup Big Data Institute (VinBigdata), code VINIF.2021.TS.019. Samples are fabricated in the cleanroom of the Nano and Energy Center. We would like to thank Dr. Pham Do Chung for help with optical measurements. Optical data are measured at VNU University of Science. Sample thicknesses are measured at Jeonbuk National University. The calculations in this work are done at the PHENIKAA University's HPC Systems.

Disclosures.

The author declare no conflicts of interest.

References

- [1] G. Schmidt, M. M. Malwitz, Properties of polymer–nanoparticle composites, *Current Opinion in Colloid and Interface Science* 8 (2003) 103–108.
- [2] G. Odegard, T. Clancy, T. Gates, Modeling of the mechanical properties of nanoparticle/polymer composites, *Polymer* 46 (2) (2005) 553–562. doi:<https://doi.org/10.1016/j.polymer.2004.11.022>. URL <https://www.sciencedirect.com/science/article/pii/S0032386104011243>
- [3] D. Guo, G. Xie, J. Luo, Mechanical properties of nanoparticles: basics and applications, *Journal of physics D: applied physics* 47 (1) (2013) 013001.
- [4] K. Chrissafis, D. Bikiaris, Can nanoparticles really enhance thermal stability of polymers? part i: An overview on thermal decomposition of addition polymers, *Thermochimica Acta* 523 (1-2) (2011) 1–24.
- [5] D. Bikiaris, Can nanoparticles really enhance thermal stability of polymers? part ii: An overview on thermal decomposition of polycondensation polymers, *Thermochimica Acta* 523 (1-2) (2011) 25–45.
- [6] M. Norouzi, Y. Zare, P. Kiany, Nanoparticles as effective flame retardants for natural and synthetic textile polymers: application, mechanism, and optimization, *Polymer Reviews* 55 (3) (2015) 531–560.
- [7] Y. Cui, S. Kumar, B. R. Kona, D. van Houcke, Gas barrier properties of polymer/clay nanocomposites, *Rsc Advances* 5 (78) (2015) 63669–63690.

- [8] C. Wolf, H. Angellier-Coussy, N. Gontard, F. Doghieri, V. Guillard, How the shape of fillers affects the barrier properties of polymer/non-porous particles nanocomposites: A review, *Journal of Membrane Science* 556 (2018) 393–418.
- [9] Y.-x. Zhang, Y.-h. Wang, Nonlinear optical properties of metal nanoparticle: a review, *RSC advances* 7 (71) (2017) 45129–45144.
- [10] M. M. Demir, K. Koynov, Ü. Akbey, C. Bubeck, I. Park, I. Lieberwirth, G. Wegner, Optical properties of composites of pmma and surface-modified zincite nanoparticles, *Macromolecules* 40 (4) (2007) 1089–1100.
- [11] N. Cioffi, L. Torsi, N. Ditaranto, G. Tantillo, L. Ghibelli, L. Sabbatini, T. Bleve-Zacheo, M. D'Alessio, P. G. Zambonin, E. Traversa, Copper nanoparticle/polymer composites with antifungal and bacteriostatic properties, *Chemistry of Materials* 17 (21) (2005) 5255–5262.
- [12] A. Liu, Z. Hong, X. Zhuang, X. Chen, Y. Cui, Y. Liu, X. Jing, Surface modification of bioactive glass nanoparticles and the mechanical and biological properties of poly (l-lactide) composites, *Acta Biomaterialia* 4 (4) (2008) 1005–1015.
- [13] R. Shenhar, T. B. Norsten, V. M. Rotello, Polymer-mediated nanoparticle assembly: structural control and applications, *Advanced Materials* 17 (6) (2005) 657–669.
- [14] J. Lu, K.-S. Moon, J. Xu, C. Wong, Synthesis and dielectric properties of novel high-k polymer composites containing in-situ formed silver nanoparticles for embedded capacitor applications, *Journal of Materials Chemistry* 16 (16) (2006) 1543–1548.
- [15] P. C. Ma, B. Z. Tang, J.-K. Kim, Effect of cnt decoration with silver nanoparticles on electrical conductivity of cnt-polymer composites, *Carbon* 46 (11) (2008) 1497–1505.
- [16] A. Ohlan, K. Singh, A. Chandra, S. Dhawan, Microwave absorption properties of conducting polymer composite with barium ferrite nanoparticles in 12.4–18 ghz, *Applied physics letters* 93 (5) (2008) 053114.
- [17] R. Pratibha, K. Park, I. I. Smalyukh, W. Park, Tunable optical metamaterial based on liquid crystal-gold nanosphere composite, *Opt. Express* 17 (22) (2009) 19459–19469. doi:10.1364/OE.17.019459. URL <https://opg.optica.org/oe/abstract.cfm?URI=oe-17-22-19459>
- [18] J. Lee, T. Javed, T. Skeini, A. O. Govorov, G. W. Bryant, N. A. Kotov, Bioconjugated ag nanoparticles and cdte nanowires: metamaterials with field-enhanced light absorption, *Angewandte Chemie* 118 (29) (2006) 4937–4941.

[19] L. Cai, Y. Peng, J. Xu, C. Zhou, C. Zhou, P. Wu, D. Lin, S. Fan, Y. Cui, Temperature regulation in colored infrared-transparent polyethylene textiles, Joule 3 (6) (2019) 1478–1486.

[20] B. C. Smith, Infrared spectral interpretation: a systematic approach, CRC press, 2018.

[21] D. Brissinger, Complex refractive index of polycarbonate over the UV-Vis-NIR region from 0.2 to 3 μm , Applied Optics 58 (6) (2019) 1341–1350. doi:10.1364/AO.58.001341. URL <https://opg.optica.org/ao/abstract.cfm?URI=ao-58-6-1341>

[22] P. T. Hong, H. Q. Nguyen, H. T. M. Nghiem, Complex refractive index measurements of poly(methyl methacrylate) (pmma) over the uv-vis-nir region, Opt. Continuum 2 (11) (2023) 2280–2289. doi:10.1364/OPTCON.495634. URL <https://opg.optica.org/optcon/abstract.cfm?URI=optcon-2-11-2280>

[23] P. Kubelka, New contributions to the optics of intensely light-scattering materials. part i, Josa 38 (5) (1948) 448–457.

[24] M. Quinten, Nanoparticle Systems and Experimental Optical Observables, John Wiley & Sons, Ltd, 2011, Ch. 2, pp. 9–36. arXiv:<https://onlinelibrary.wiley.com/doi/pdf/10.1002/9783527633135.ch2>, doi:<https://doi.org/10.1002/9783527633135.ch2>. URL <https://onlinelibrary.wiley.com/doi/abs/10.1002/9783527633135.ch2>

[25] M. I. Mishchenko, G. Videen, P. Yang, Extinction by a homogeneous spherical particle in an absorbing medium, Opt. Lett. 42 (23) (2017) 4873–4876. doi:10.1364/OL.42.004873. URL <https://opg.optica.org/ol/abstract.cfm?URI=ol-42-23-4873>

[26] G. Latour, M. Elias, J.-M. Frigerio, Determination of the absorption and scattering coefficients of pigments: Application to the identification of the components of pigment mixtures, Appl. Spectrosc. 63 (6) (2009) 604–610. URL <https://opg.optica.org/as/abstract.cfm?URI=as-63-6-604>

[27] D. Barrios, R. Vergaz, J. M. Sanchez-Pena, C. G. Granqvist, G. A. Niklasson, Toward a quantitative model for suspended particle devices: Optical scattering and absorption coefficients, Solar Energy Materials and Solar Cells 111 (2013) 115–122. doi:<https://doi.org/10.1016/j.solmat.2012.12.012>. URL <https://www.sciencedirect.com/science/article/pii/S0927024812005429>

[28] J. Wang, C. Xu, A. M. Nilsson, D. L. Fernandes, M. Strömberg, J. Wang, G. A. Niklasson, General method for determining light scattering and absorption of nanoparticle composites, Advanced Optical Materials 7 (4) (2019) 1801315.

[29] J. Wang, A. M. Nilsson, D. Barrios, W. E. Vargas, E. Wäckelgård, G. A. Niklasson, Light scattering materials for energy-related applications: Determination of absorption and scattering coefficients, *Materials Today: Proceedings* 33 (2020) 2474–2480. doi:<https://doi.org/10.1016/j.matpr.2020.01.339>. URL <https://www.sciencedirect.com/science/article/pii/S2214785320304387>

[30] J. Nobbs, Kubelka—munk theory and the prediction of reflectance, *Review of Progress in Coloration and Related Topics* 15 (2008) 66 – 75. doi:10.1111/j.1478-4408.1985.tb03737.x.

[31] W. M. Star, J. P. A. Marijnissen, M. J. C. van Gemert, Light dosimetry in optical phantoms and in tissues: I. multiple flux and transport theory, *Physics in Medicine & Biology* 33 (4) (1988) 437. doi:10.1088/0031-9155/33/4/004. URL <https://dx.doi.org/10.1088/0031-9155/33/4/004>

[32] S. N. Thennadil, Relationship between the kubelka-munk scattering and radiative transfer coefficients, *J. Opt. Soc. Am. A* 25 (7) (2008) 1480–1485. doi:10.1364/JOSAA.25.001480. URL <https://opg.optica.org/josaa/abstract.cfm?URI=josaa-25-7-1480>

[33] C. Sandoval, A. D. Kim, Deriving kubelka-munk theory from radiative transport, *J. Opt. Soc. Am. A* 31 (3) (2014) 628–636. doi:10.1364/JOSAA.31.000628. URL <https://opg.optica.org/josaa/abstract.cfm?URI=josaa-31-3-628>

[34] C. F. Bohren, D. R. Huffman, *Absorption and scattering of light by small particles*, John Wiley & Sons, 2008.

[35] G.-h. Wang, Y. Zhang, D.-h. Zhang, J.-p. Fan, Design and calculation of low infrared transmittance and low emissivity coatings for heat radiative applications, *International Journal of Minerals, Metallurgy, and Materials* 19 (2012). doi:10.1007/s12613-012-0535-0.

[36] M. S. Wheeler, J. S. Aitchison, J. I. Chen, G. A. Ozin, M. Mojahedi, Infrared magnetic response in a random silicon carbide micropowder, *Physical Review B* 79 (7) (2009) 073103.

[37] W. C. Mundy, J. A. Roux, A. M. Smith, Mie scattering by spheres in an absorbing medium*, *J. Opt. Soc. Am.* 64 (12) (1974) 1593–1597. doi:10.1364/JOSA.64.001593. URL <https://opg.optica.org/abstract.cfm?URI=josa-64-12-1593>

[38] P. Chýlek, Light scattering by small particles in an absorbing medium*, *J. Opt. Soc. Am.* 67 (4) (1977) 561–563. doi:10.1364/JOSA.67.000561. URL <https://opg.optica.org/abstract.cfm?URI=josa-67-4-561>

[39] C. F. Bohren, D. P. Gilra, Extinction by a spherical particle in an absorbing medium, *Journal of Colloid and Interface Science* 72 (2) (1979) 215–221. doi:[https://doi.org/10.1016/0021-9797\(79\)90103-6](https://doi.org/10.1016/0021-9797(79)90103-6).
URL <https://www.sciencedirect.com/science/article/pii/0021979779901036>

[40] M. Quinten, J. Rostalski, Lorenz-mie theory for spheres immersed in an absorbing host medium, *Particle & Particle Systems Characterization* 13 (2) (1996) 89–96. doi:<https://doi.org/10.1002/ppsc.19960130206>.
URL <https://onlinelibrary.wiley.com/doi/abs/10.1002/ppsc.19960130206>

[41] Lebedev, A. N., Gartz, M., Kreibig, U., Stenzel, O., Optical extinction by spherical particles in an absorbing medium: Application to composite absorbing films, *Eur. Phys. J. D* 6 (3) (1999) 365–373. doi:[epjd/v6/p365\(d8252\)](https://doi.org/epjd/v6/p365(d8252)).
URL [https://doi.org/epjd/v6/p365\(d8252\)](https://doi.org/epjd/v6/p365(d8252))

[42] I. W. Sudiarta, P. Chylek, Mie-scattering formalism for spherical particles embedded in an absorbing medium, *J. Opt. Soc. Am. A* 18 (6) (2001) 1275–1278. doi:[10.1364/JOSAA.18.001275](https://doi.org/10.1364/JOSAA.18.001275).
URL <https://opg.optica.org/josaa/abstract.cfm?URI=josaa-18-6-1275>

[43] M. Gnanavel, T. Maridurai, K. Kumar, Mechanical, thermal and dielectric behaviour of c-class fly-ash coarse and fine particles reinforced epoxy resin composite, *Materials Research Express* 6 (9) (2019) 095507.

[44] A. Ishimura, *Wave Propagation and Scattering in Random Media*, Academic Press, 1978. doi:<https://doi.org/10.1016/B978-0-12-374701-3.X5001-7>.

[45] J. L. Saunderson, Calculation of the color of pigmented plastics*, *J. Opt. Soc. Am.* 32 (12) (1942) 727–736. doi:[10.1364/JOSA.32.000727](https://doi.org/10.1364/JOSA.32.000727).
URL <https://opg.optica.org/abstract.cfm?URI=josa-32-12-727>

[46] W. E. Vargas, G. A. Niklasson, Applicability conditions of the kubelka–munk theory, *Appl. Opt.* 36 (22) (1997) 5580–5586. doi:[10.1364/AO.36.005580](https://doi.org/10.1364/AO.36.005580).
URL <https://opg.optica.org/ao/abstract.cfm?URI=ao-36-22-5580>

[47] I. Hughes, T. Hase, *Measurements and their uncertainties: a practical guide to modern error analysis*, OUP Oxford, 2010.
URL <https://global.oup.com/ukhe/product/measurements-and-their-uncertainties-9780199566334?cc=vn>

[48] Y. Zhai, Y. Ma, S. N. David, D. Zhao, R. Lou, G. Tan, R. Yang, X. Yin, Scalable-manufactured randomized glass-polymer hybrid metamaterial for daytime radiative cooling, *Science* 355 (6329) (2017) 1062–1066. doi:[10.1126/science.aal2700](https://doi.org/10.1126/science.aal2700).

1126/science.aai7899.

URL <https://www.science.org/doi/abs/10.1126/science.aai7899>

[49] J. Mandal, Y. Fu, A. C. Overvig, M. Jia, K. Sun, N. N. Shi, H. Zhou, X. Xiao, N. Yu, Y. Yang, Hierarchically porous polymer coatings for highly efficient passive daytime radiative cooling, *Science* 362 (6412) (2018) 315–319. doi:10.1126/science.aat9513.

URL <https://www.science.org/doi/abs/10.1126/science.aat9513>

Supplementary Material on "Absorption and scattering properties of nanoparticles in an absorbing medium: revisiting with experimental validation"

1. Technical data of TiO_2 particles

The size of TiO_2 nanoparticles in this research is measured with a dynamic light scattering apparatus using Zeta sizer Nano S equipment, Malvern. TiO_2 nanoparticles are dispersed in a water medium by ultrasonic vibration within 4 hours at 25 $^{\circ}\text{C}$. We perform three continuous measurements to collect the average diameter spectra of TiO_2 nanoparticles with two radii, as presented in Fig. S1. We use a log-normal distribution to describe the size of TiO_2 nanoparticles expressed by

$$\rho(a) = \frac{1}{a\sigma\sqrt{2\pi}} \exp\left(-\frac{(\ln a - \mu)^2}{2\sigma^2}\right). \quad (\text{S1})$$

Here, a is the particle radius, μ , and σ are determined from the values of mean and mode, given by

$$\mu = [\ln(\text{mode}) + 2\ln(\text{mean})]/3, \quad (\text{S2})$$

$$\sigma^2 = 2/3[\ln(\text{mean}) - \ln(\text{mode})]. \quad (\text{S3})$$

Both mean and mode are the experimental results of size measurements. From those results, the average radius of the two types of TiO_2 nanoparticles is 15nm in the blue line and 55nm in the red line in Fig. S1. Hence, we use these results in the experimental and theoretical calculation of thin-film composites.

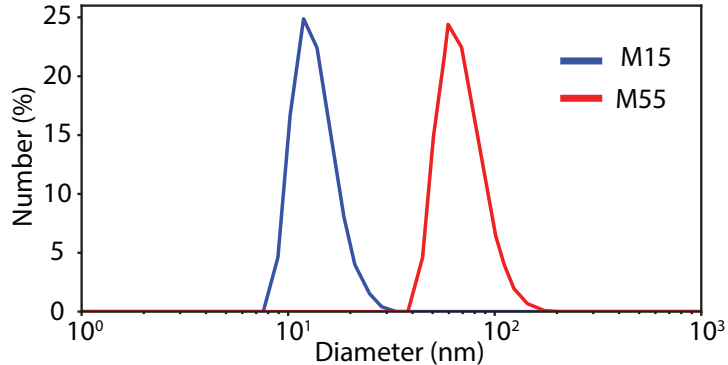


Figure S1: **Information of TiO_2 nanoparticles:** the particle size distribution of two types of TiO_2 nanoparticles by dynamic light scattering.

2. Reflection at front and back interfaces of thin-film composites

When light passes through thin-film composites, it can undergo reflection at both the front and back interface of the film. Determining these reflections is necessary for the two-flux Kubleka-Munk theory [S1]. The frontside internal reflectance of the film is denoted by R_j , while the backside internal reflectance is represented by R_g . They are dependent on the fraction of diffused light q_j and q_g [S2, S3], expressed by

$$R_j = (1 - q_j)R_c + q_jR_d, \quad (S4)$$

$$R_g = (1 - q_g)R_c + q_gR_d, \quad (S5)$$

in which R_c indicates the fraction of collimated light reflected at the front interface determined in our previous report [S4] in the black in Fig. S2, while R_d is the diffused reflection in the blue in Fig. S2. In our thin-film composite, an isotropic light scattering profile is considered in both forward and backward directions at angles smaller than the critical angle. Since the particles are at the nanometer scale, the diffused reflection R_d is determined using the critical approximation [S2]. Hence,

$$R_d = \frac{\int_0^{\theta_c} R(\theta) \sin(\theta) \cos(\theta) d\theta}{\int_0^{\theta_c} \sin(\theta) \cos(\theta) d\theta}, \quad (S6)$$

in which $\theta_c = \arcsin(1/n_h)$ is the wavelength-dependent critical angle, n_h is refractive index of PMMA. $R(\theta)$ is the reflection of the PMMA medium at the front internal interfaces depending on the incident angle [S5], given by

$$R_\theta = \frac{R_{\parallel}(\theta) + R_{\perp}(\theta)}{2}, \quad (S7)$$

$$R_{\parallel}(\theta) = \frac{\cos(\theta)/\cos(\chi) - (n_h - i\kappa_h)/(n_{\text{air}} - i\kappa_{\text{air}})}{\cos(\theta)/\cos(\chi) + (n_h - i\kappa_h)/(n_{\text{air}} - i\kappa_{\text{air}})}, \quad (S8)$$

$$R_{\perp}(\theta) = \frac{\cos(\chi)/\cos(\theta) - (n_h - i\kappa_h)/(n_{\text{air}} - i\kappa_{\text{air}})}{\cos(\chi)/\cos(\theta) + (n_h - i\kappa_h)/(n_{\text{air}} - i\kappa_{\text{air}})} \quad (S9)$$

in which θ is the incident angle, while χ is the refraction angle. (n_h, κ_h) and $(n_{\text{air}}, \kappa_{\text{air}})$ are the refractive index of PMMA medium and air medium, respectively. Fig. S2 shows the collimated and diffused reflection at the two interfaces of the thin-film composites with three concentrations: 0.5% in green, 1% in red, and 5% in purple. The backside internal reflectance R_g increases following the mass concentration, which range from R_c to R_d .

3. Investigation of the $K - S$ possible values

The values of the fractions of diffuse light at the frontside and backside interfaces, q_j and q_g , are necessary for extracting the absorption K and scattering S coefficient of nanoparticle in the polymer. However, two parameters can not

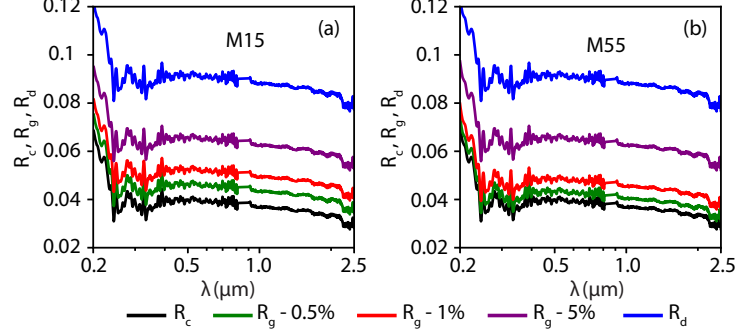


Figure S2: **Collimated and diffused reflection:** series M15 in (a), and series M55 in (b). R_c is the specular reflection of collimated light at the front interface in the black line, while R_d in the blue line indicates the reflection of diffused light calculated by equation S6. The backside internal reflectance R_g is determined by equation S5 with three mass concentrations: 0.5% in the green line, 1% in the red line, and 5% in the purple line.

measured directly in this research. Therefore, we examine the possible values of K and S from measured data R and T at $\lambda = 0.5 \mu m$ by changing the values of $q_{j,g}$ from 0 to 1. The top row in Fig. S3 shows the heatmap of q_g and q_j values in series M15, while the bottom row shows these values in series M55 with three concentrations of mass of TiO_2 nanoparticles: 0.5%, 1%, and 5%. The cyan contour lines are the values of $(K + S)$ corresponding with the possible values of q_g and q_j at $\lambda = 0.5 \mu m$. Based on the heatmap, we note that the value of q_j is approximately greater than q_g about 2 times since the light goes the double distance from the front to back interface and back leading to an increase in the number of times light encounters the particle. Therefore, we presume that $q_j \approx 2q_g$ and do not exceed 1 in all cases with different concentrations. Increasing the mass concentration of TiO_2 nanoparticles in PMMA medium makes the expansion of the values of q_g and q_j . Based on the heatmap of q_g and q_j values, the $(K + S)$ are non-negative in the acceptable range.

4. Effective refractive index of the particulate medium

The optical properties of PMMA are shown in Figs. S4a. The refractive index of PMMA is studied in our previous research [S22] due to the lack of data on the UV regime. Fig. S4b is the refractive index of TiO_2 adapted from Ref. [S6]. When TiO_2 dispersed in PMMA medium, the thin-film composites become a particulate medium with refractive index (n_{eff}, κ_{eff}) . It represents the mean effect of other particles inside the composite on a given particle, which is expressed through the effective permittivity ε_{eff} and permeability μ_{eff} [S7, S8],

$$n_{eff} + i\kappa_{eff} = \sqrt{\varepsilon_{eff}\mu_{eff}}. \quad (S10)$$

In which the effective permittivity ε_{eff} and permeability μ_{eff} are associated with the forward and backward scattering amplitudes of particles hosted in the ma-

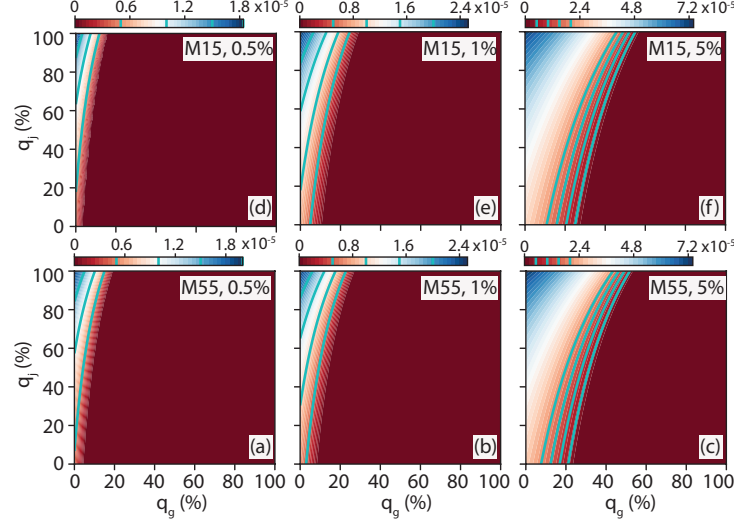


Figure S3: **Heatmap of q_g and q_j values:** series M15 in (a-c), series M55 in (d-e) with three different concentrations: 0.5%, 1%, and 5%. The color bar describes the values of $(K + S)$, and the contour line in cyan is the $(K + S)$ values corresponding with the possible values of q_g and q_j based on the measured data.

trix, $S(a, 0)$ and $S(a, \pi)$ [S9]. They are given by

$$\varepsilon_{\text{eff}} = \varepsilon_0 \frac{1 + (2/3)\gamma}{1 - \gamma/3}, \quad (\text{S11})$$

$$\mu_{\text{eff}} = \frac{1 + (2/3)\delta}{1 - \delta/3}, \quad (\text{S12})$$

here ε_0 is the permittivity of the PMMA matrix calculated from n_h and k_h , and

$$\begin{aligned} \gamma &= \int \frac{3i}{2\bar{x}^3} \left[N_p \frac{4\pi}{3} a^3 \rho(a) \right] [S(a, 0) + S(a, \pi)] da, \\ \delta &= \int \frac{3i}{2\bar{x}^3} \left[N_p \frac{4\pi}{3} a^3 \rho(a) \right] [S(a, 0) - S(a, \pi)] da, \end{aligned}$$

where N_p is the particle density, a is the particle radius, $\rho(a)$ is the particle size distribution, $\bar{x} = 2\pi(n_h + ik_h)a/\lambda$ is the size parameter.

Fig. S4c of series M15 and Fig. S4d of series M55 show the refractive index of a particular medium with four concentrations: 0% in black, 0.5% in green, 1% in red, and 5% in purple. The refractive index n_{eff} of the particulate medium in the solid line is similar to that of PMMA. It means that the refractive index is not affected by particles in all samples. In contrast, the effective extinction coefficient κ_{eff} in the dashed line increases following the TiO_2 particle concentrations, which is higher than that of PMMA. In the calculation of the Mie cross-sections, the optical properties of the surrounding medium affect the absorption and scattering of individual particles.

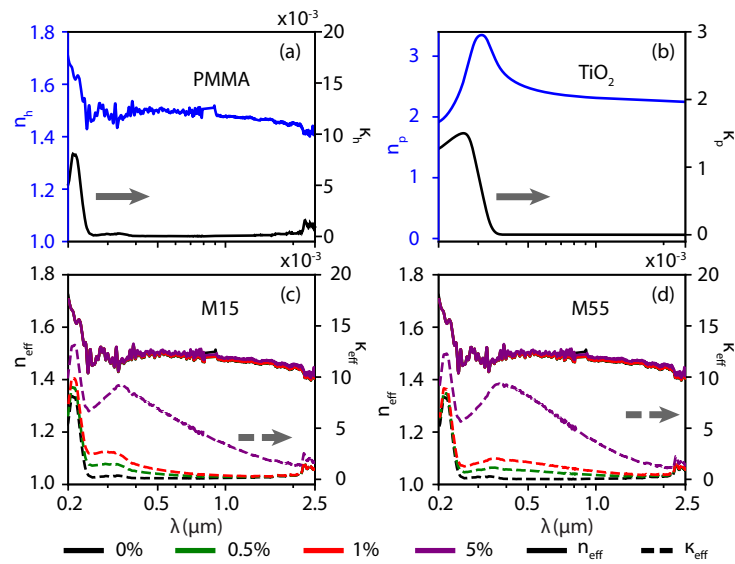


Figure S4: **Complex refractive index:** (a) refractive index and extinction coefficient of PMMA in our previous research [S4], and (b) TiO_2 adapted from Ref. [S6]. The particulate medium with refractive index n_{eff} in solid line and extinction coefficient κ_{eff} are presented in (c) of series M15 and in (d) of series M55 with different concentrations.

References

- [S1] P. Kubelka, New contributions to the optics of intensely light-scattering materials. part i, *Josa* 38 (5) (1948) 448–457.
- [S2] J. Wang, C. Xu, A. M. Nilsson, D. L. Fernandes, M. Strömberg, J. Wang, G. A. Niklasson, General method for determining light scattering and absorption of nanoparticle composites, *Advanced Optical Materials* 7 (4) (2019) 1801315.
- [S3] J. Wang, A. M. Nilsson, D. Barrios, W. E. Vargas, E. Wäckelgård, G. A. Niklasson, Light scattering materials for energy-related applications: Determination of absorption and scattering coefficients, *Materials Today: Proceedings* 33 (2020) 2474–2480. doi:<https://doi.org/10.1016/j.matpr.2020.01.339>.
URL <https://www.sciencedirect.com/science/article/pii/S2214785320304387>
- [S4] P. T. Hong, H. Q. Nguyen, H. T. M. Nghiem, Complex refractive index measurements of poly(methyl methacrylate) (pmma) over the uv-vis-nir region, *Opt. Continuum* 2 (11) (2023) 2280–2289. doi:10.1364/OPTCON.495634.
URL <https://opg.optica.org/optcon/abstract.cfm?URI=optcon-2-11-2280>
- [S5] J. R. Howell, M. P. Mengüç, K. Daun, R. Siegel, *Thermal radiation heat transfer*, CRC press, 2020.
- [S6] T. Siefke, S. Kroker, K. Pfeiffer, O. Puffky, K. Dietrich, D. Franta, I. Ohlídal, A. Szeghalmi, E.-B. Kley, A. Tünnermann, Materials pushing the application limits of wire grid polarizers further into the deep ultraviolet spectral range, *Advanced Optical Materials* 4 (11) (2016) 1780–1786.
- [S7] W. E. Vargas, G. A. Niklasson, Applicability conditions of the kubelka–munk theory, *Appl. Opt.* 36 (22) (1997) 5580–5586. doi:10.1364/AO.36.005580.
URL <https://opg.optica.org/ao/abstract.cfm?URI=ao-36-22-5580>
- [S8] M. S. Wheeler, J. S. Aitchison, J. I. Chen, G. A. Ozin, M. Mojahedi, Infrared magnetic response in a random silicon carbide micropowder, *Physical Review B* 79 (7) (2009) 073103.
- [S9] C. Bohren, D. Huffman, *Absorption and Scattering of Light by Small Particles*, Wiley Science Series, John Wiley & Sons, 2008, Ch. 4, pp. 82–129.
URL <https://books.google.com.vn/books?id=ib3EMXXIRXUC>